PIN WITHOUT HEAD HR-18152 - TIN BRONZE - LATE BRONZE AGE - SWITZERLAND

Artefact name	Pin without head HR-18152
Authors	Marianne. Senn (Empa, Dübendorf, Zurich, Switzerland) & Christian. Degrigny (HE-Arc CR, Neuchâtel, Neuchâtel, Switzerland) & Naima. Gutknecht (HE-Arc CR, Neuchâtel, Neuchâtel, Switzerland) & Rémy. Léopold (HE-Arc CR, Neuchâtel, Neuchâtel, Switzerland)
Url	/artefacts/1350/

The object

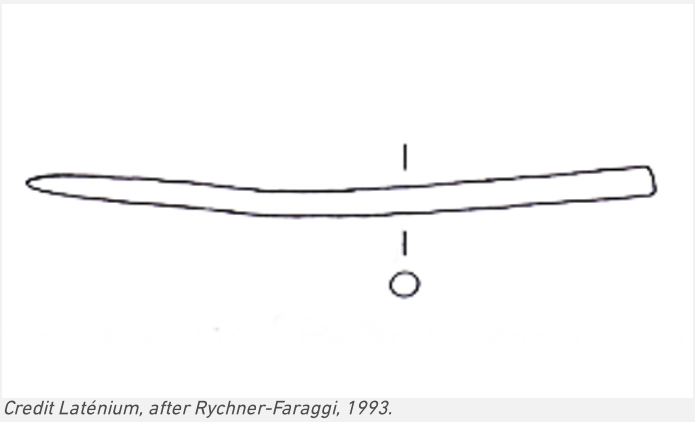

Credit Laténium, after Rychner-Faraggi, 1993.

Fig. 1: Pin without head (after Rychner-Faraggi 1993, plate 74.29),

Credit Laténium, C.Cevey.

Fig. 2: Dense and smooth brown-yellow corrosion product (detail) of the pin,

Description and visual observation

Description of the artefact	Pin without head and smooth brown-yellow corrosion products (Figs. 1-2). Dimensions: L = 7,5cm; Ø = 3.3mm; WT = 4g.
Type of artefact	Jewellery
Origin	Hauterive - Champréveyres, Neuchâtel, Neuchâtel, Switzerland
Recovering date	Excavation 1983-1985, object from layer 3 to 5
Chronology category	Late Bronze Age
chronology tpq	1054 B.C.
chronology taq	1000 B.C.
Chronology comment	Hallstatt B1 (1054/1037BC _ 1000BC)
Burial conditions / environment	Lake

Artefact location	Laténium, Neuchâtel, Neuchâtel
Owner	Laténium, Neuchâtel, Neuchâtel
Inv. number	HR 18152
Recorded conservation data	N/A

Complementary information

The object was sampled in 1987 for analysis by Schweizer. Documentation of the strata in binocular mode on the remaining fragment of the object was performed in 2022.

Study area(s)

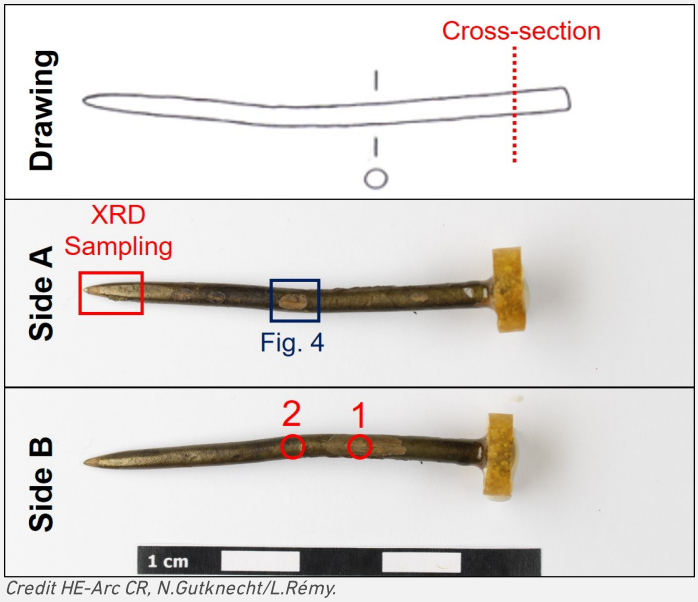

Credit HE-Arc CR, N.Gutknecht/L.Rémy.

Fig. 3: Location of cross-section on drawing before sampling and sides A and B (opposite sides) with indication of XRF analyses (red circles), XRD sampling (red square) and Fig. 4 (blue square),

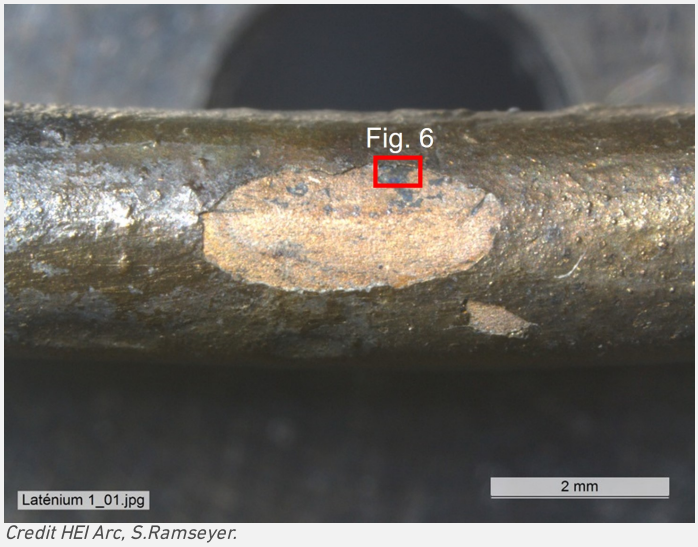

Credit HEI Arc, S.Ramseyer.

Fig. 4: Lacuna showing the underlying metal with location of Fig. 6 (red rectangle),

Fig. 5: Side view of a lacuna with the stratigraphy of the brown-yellow corrosion layer,

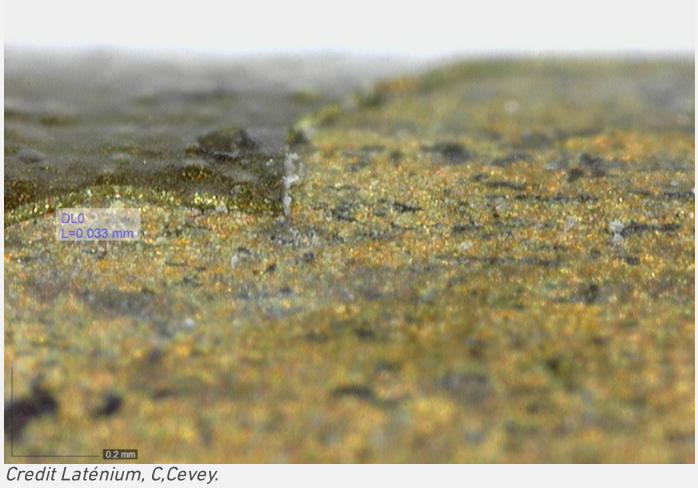

Credit Laténium, C,Cevey.

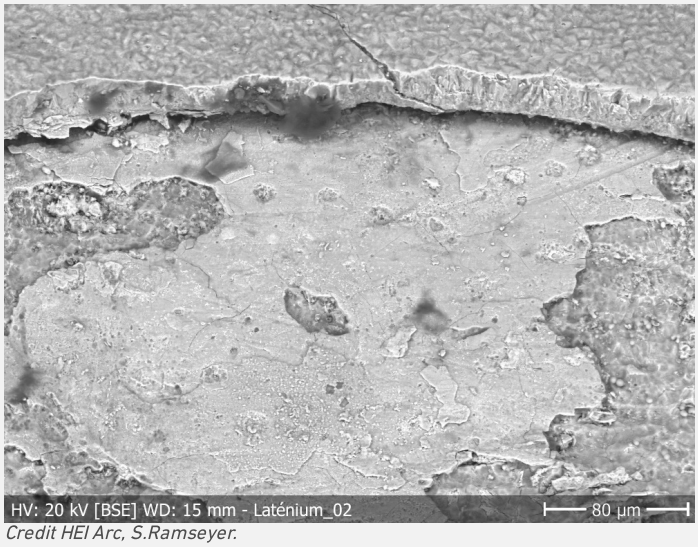

Credit HEI Arc, S.Ramseyer.

Fig. 6: SEM image of the pin from Fig. 4 (detail), BSE-mode. The crack between the remaining metal and the corrosion layers is clearly visible. The smooth layer below is CP3 (see below),

Binocular observation and representation of the corrosion structure

The schematic representation below gives an overview of the corrosion structure encountered on the pin from a first visual macroscopic observation.

Strata	Type of stratum	Principal characteristics
CP1	Corrosion product	Layer, olive green, metallic, medium thickness, compact, tough, soft
CP2	Corrosion product	Nodule, light green, thin, scattered, non compact, powdery, very soft
CP3	Corrosion product	Black, thin, scattered, compact, friable, soft
M1	Metal	Dark yellow, thick, continuous, compact, tough, soft

Table 1: Description of the principal characteristics of the strata as observed under binocular and described according to Bertholon's method.

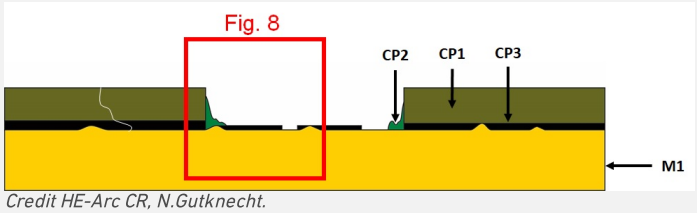

Credit HE-Arc CR, N.Gutknecht.

Fig. 7: Stratigraphic representation of the corrosion structure of the pin without head by macroscopic and binocular observation with indication of the corrosion structure used to build the MiCorr stratigraphy of Fig. 8 (red square),

MiCorr stratigraphy(ies) – Bi

Fig. 8: Stratigraphic representation of the corrosion structure of the pin without head observed macroscopically under binocular microscope using the MiCorr application with reference to Fig. 7. The characteristics of the strata, such as

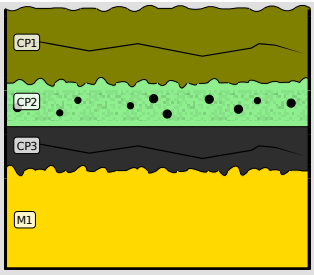

discontinuity, are accessible by clicking on the drawing that redirects you to the search tool by stratigraphy representation, Credit HE-Arc CR, N.Gutknecht.

Sample(s)

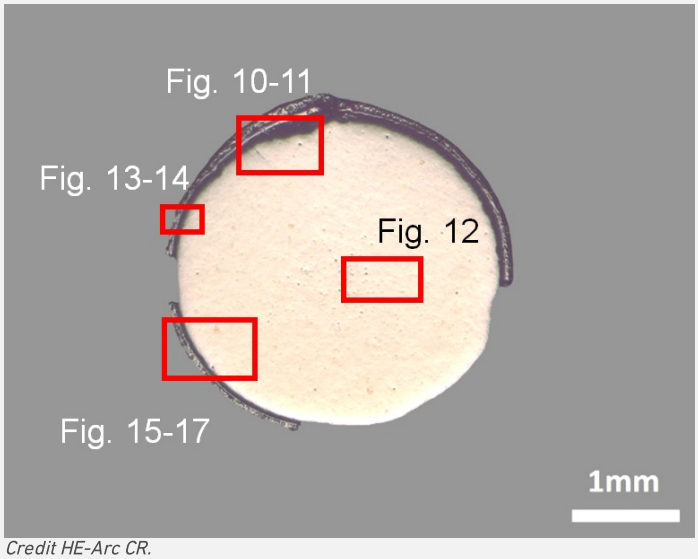

Credit HE-Arc CR.

Fig. 9: Micrograph of the cross-section of the sample taken from the pin without head showing the location of Figs. 10 to 17,

Description of sample	The cross-section is circular and is a complete section through the pin (Fig. 3). It is covered with a rather thin and regular (in thickness) corrosion layer (Fig. 6). On the sample, one third of the corrosion layer is missing (Fig. 9).
Alloy	Tin Bronze
Technology	Annealed after cold working
Lab number of sample	MAH 87-194
Sample location	Laténium, Neuchâtel, Neuchâtel
Responsible institution	Laténium, Neuchâtel, Neuchâtel
Date and aim of sampling	1987, metallography and corrosion characterisation

Complementary information

This sample is mentioned in Schweizer, 1994. It was taken in 1987 and there is no photographic documentation of the object before cutting and sampling.

Analyses and results

Analyses performed:

Non-invasive approach

XRF with handheld portable X-ray fluorescence spectrometer (NITON XL5). General Metal mode, acquisition time 60s (filters: Li20/Lo20/M20).

Invasive approach (on the sample)

Metallography (etched with ferric chloride reagent), Vickers hardness testing, XRF, ICP-OES, SEM/EDS, XRD, Raman spectroscopy (conditions provided in the About tab of the MiCorr application).

Non invasive analysis

XRF analyses of the pin were carried out on two representative areas (Fig. 3). Point 1 was done in a lacuna of the brown-yellow corrosion layer, while point 2 was performed on the brown corrosion layer (CP1) where all strata (soil, corrosion products, and metal) are analyzed at the same time.

The metal is presumably a tin bronze alloy. The other elements detected are : S, Fe, Si, Al, Pb, Sb, As, Ag, Zn, Ni.

Results of point 2 are very different from those of point 1, they indicate the surface enrichment in Fe and in S and the depletion in Cu.

Elements (mass %)	Cu		Sn		S		Fe		Si		Al		Pb		Sb		As		Ag		Zn		Ni	
	%	+/-2σ	%	+/-2σ	%	+/-2σ	%	+/-2σ	%	+/-2σ	%	+/-2σ	%	+/-2σ	%	+/-2σ	%	+/-2σ	%	+/-2σ	%	+/-2σ	%	+/-2σ
1	78.5	0.13	7.5	0.04	6.5	0.05	4.0	0.04	1.5	0.01	0.5	0.11	0.2	0.01	0.2	0.01	0.2	0.02	0.1	0.02	<0.1	<0.01	<0.1	0.01
2	39.0	0.1	5.0	0.03	26.0	0.08	30.0	0.08	0.3	0.03	<LD	<LD	<0.1	0.01	0.1	0.01	<0.1	0.01	<0.1	0.02	0.1	0.02	<LD	<LD

Table 2: Chemical composition of the surface of the pin at two representative points shown in Fig. 3. Method of analysis: XRF, UR-Arc CR.

Metal

ICP-OES analyses of the remaining metal show a tin bronze as suggested in Table 1 (point 1). The metal also has copper sulphide as well as heavy metal (Pb-rich) inclusions (Figs. 10 and 11). Close to the surface of the remaining metal, copper sulphide inclusions are elongated and form rows (Fig. 10). The etched structure of the tin bronze shows polygonal grains; some of them are twinned (Fig. 12). In the centre of the sample and on the edges, the grains are smaller. The copper sulphide inclusions are located at the grain boundaries and in the grains. The average hardness of the metal is about HV1 110.

Elements	Cu	Sn	Pb	Sb	As	Ag	Fe	Ni	Co	Zn
mass%	89.22	9.57	0.34	0.26	0.19	0.15	0.09	0.05	0.06	0.05

Table 3: Chemical composition of the metal. Method of analysis: ICP-OES, Laboratory of Analytical Chemistry, Empa.

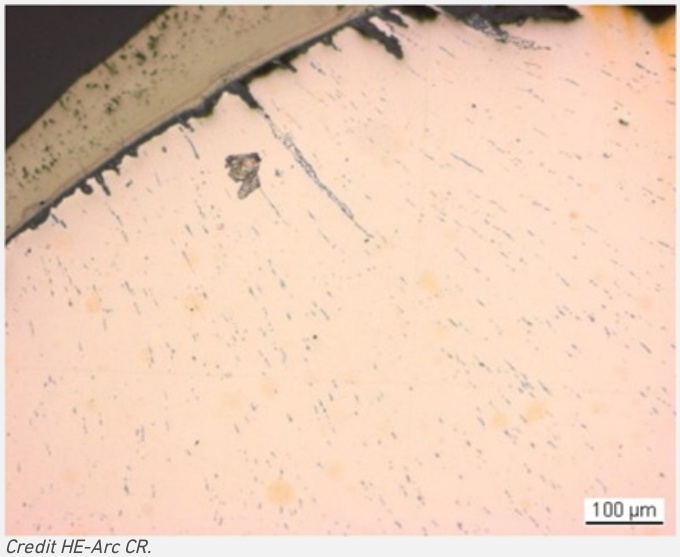

Credit HE-Arc CR.

Fig. 10: Micrograph of the metal sample from Fig. 9 (detail), unetched, bright field. Rows of elongated copper sulphide inclusions can be observed,

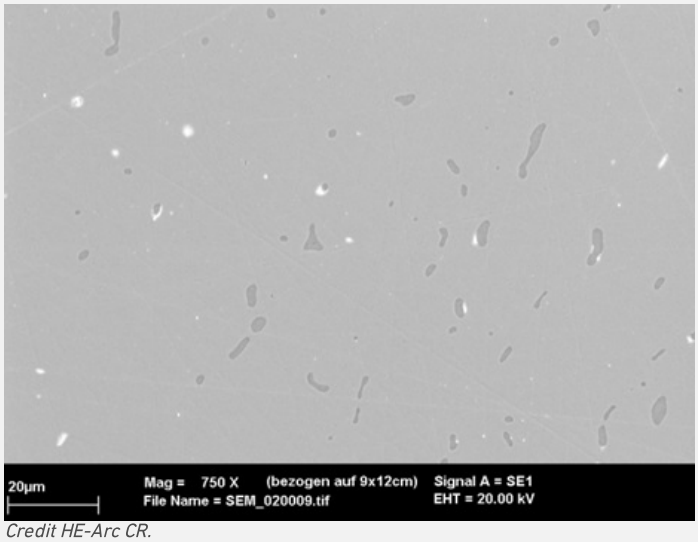

Credit HE-Arc CR.

Fig. 11: SEM image of the metal sample from Fig. 9 (detail), SE-mode. Elongated copper sulphide inclusions (dark-grey) are visible as well as heavy metal (Pb-rich) inclusions (white),

Fig. 12: Micrograph of the metal sample from Fig. 9 (detail), etched, bright field. The metal shows a structure of polygonal and twinned grains. Copper sulphide

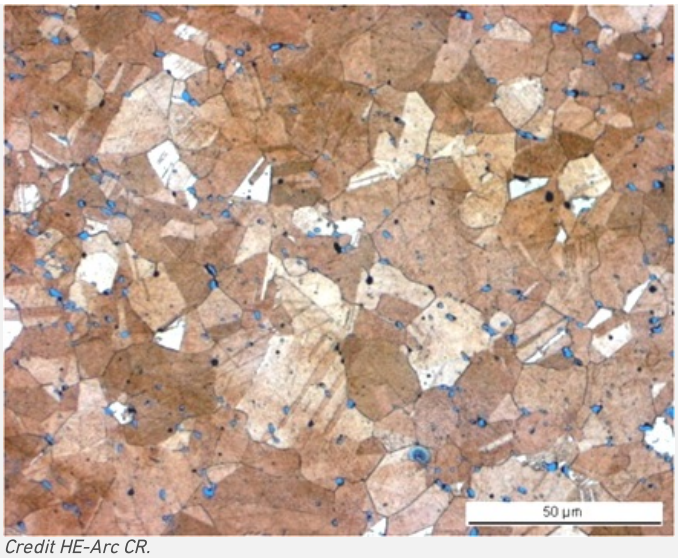

Credit HE-Arc CR.

inclusions are visible as blue spots,

Microstructure	Polygonal and twinned grains
First metal element	Cu
Other metal elements	As, Ag, Sn, Sb, Pb

Complementary information

Schweizer (1994) indicates that the copper-tin alloys similar to the one of the pin have minor constituents that were certainly not added intentionally. Furthermore, he mentions that there is no systematic composition difference between bronzes with a lake patina and those with a land patina.

Corrosion layers

The corrosion layer is regular in thickness (around 50µm, Figs. 5 and 6). It presents lacuna (Fig. 4) and in some areas it is missing completely. At the metal - corrosion layer interface, there is a crack showing that the latter has separated from the metal core along its whole length (Figs. 6, 9, 10, 13 and 14). The corrosion layer can be divided into three distinct strata (CP1-3): directly above the crack is a first dense but cracked and irregular inner layer (CP3, Figs. 6, 13 and 14). In bright field it appears brown (Fig. 15), in normal and polarised light dark brown (Fig. 16). It is separated from the adjacent layer by a clear line (Figs. 14 and 15). The second layer (CP2) is dense with little porosity (Figs. 13 and 14). In bright field it appears light brown (Fig. 15), in polarised light dark yellow (Fig. 16). The third and outermost layer (CP1) appears light brown under normal light (Fig. 2) and in bright field (Fig. 15), contains particles (Fig. 14) and is very porous (visible as golden reflections under polarized light, Fig. 16).

These results are entirely consistent with Schweizer's observations (Schweizer 1994). The elemental chemical distribution of the SEM image selected reveals that the inner layer (CP3) is depleted in Cu, but rich in Sn,O and Si (Fig. 17 and Table 4) and its interface with the intermediate layer (CP2) could represent the limit of the original surface (Figs. 14 and 17). The second and third layer (CP2 and CP1) are Fe, Cu and S-rich (Fig. 17) and have a composition similar to chalcopyrite/CuFeS2 as suggested in Table 2 (point 2). This was confirmed by XRD. The particles (inclusions) have a composition similar to covelline or covellite/CuS (Table 4). Both chalcopyrite and covelline have been identified by Raman spectroscopy (Figs. 18 and 19).

Elements	S	Fe	Cu	O	Si	Sn	Total
CP1 and CP2	35	30	34	<	<	<	**99**
Particles in CP1	26	4.1	68	<	<	<	**98**
CP3	5.8	5.0	13	32	2	41	**99**

Table 4: Chemical composition (mass %) of the corrosion layers from Fig. 15. Method of analysis: SEM/EDS, Laboratory of Analytical Chemistry, Empa.

Fig. 13: SEM image of the metal sample from Fig. 9 (detail), SE-mode. The crack between the remaining metal and the corrosion layers is clearly visible,

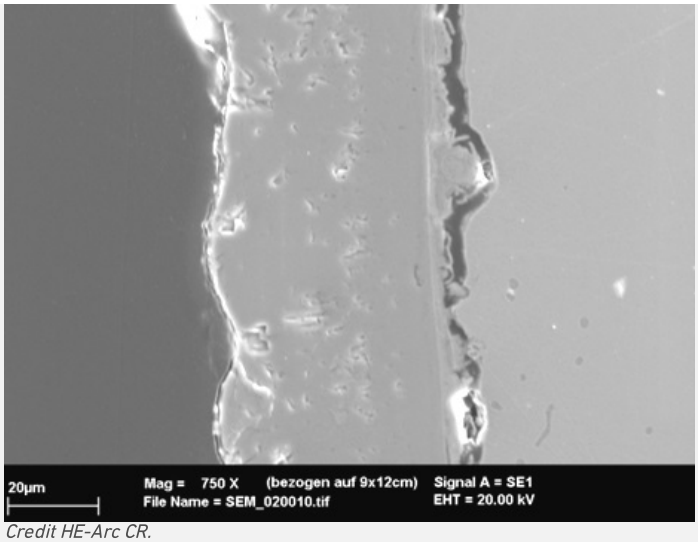

Credit HE-Arc CR.

Fig. 14: SEM image similar to Fig. 13, BSE-mode. A thin line is visible (white arrow) differentiating the inner Sn-rich layer from the intermediate and outer chalcopyrite layers. The latter contains bright covelline inclusions (black arrow) and pores,

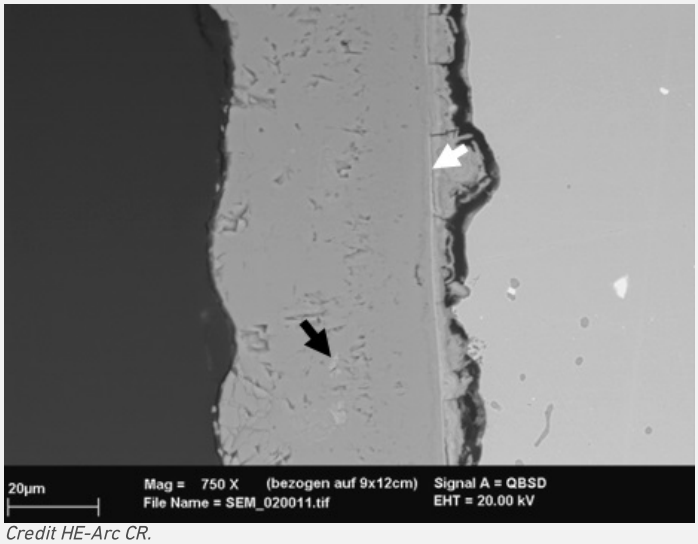

Credit HE-Arc CR.

Fig. 15: Micrograph of the metal sample from Fig. 9 (detail) and corresponding to the stratigraphy of Fig. 20, unetched, bright field. The area selected for elemental chemical distribution (Fig. 17) is marked by a red rectangle,

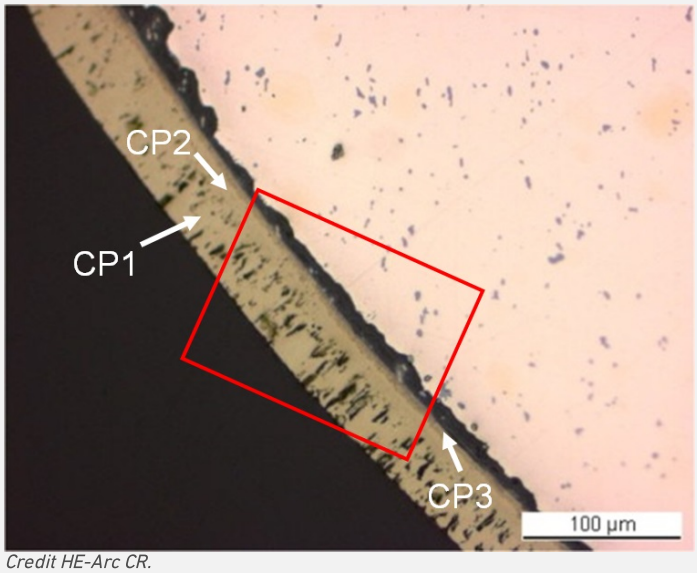

Credit HE-Arc CR.

Fig. 16: Micrograph similar to Fig. 15, polarised light,

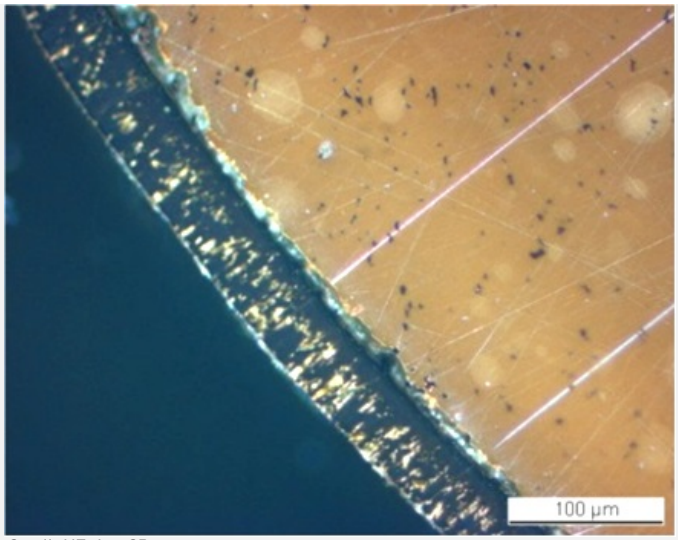

Credit HE-Arc CR.

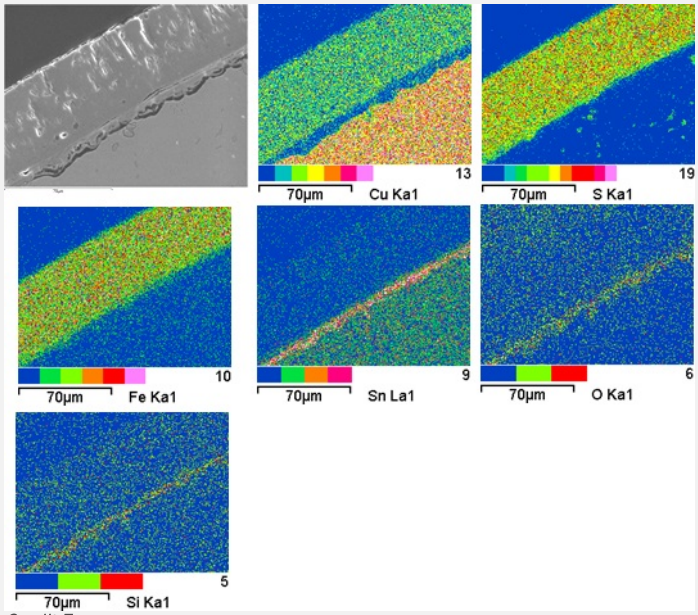

Credit Empa.

Fig. 17: SEM image and elemental chemical distribution of a selected area of Fig. 15 (rotated by 90°). Method of examination: SEM/EDS, Laboratory of Analytical Chemistry, Empa,

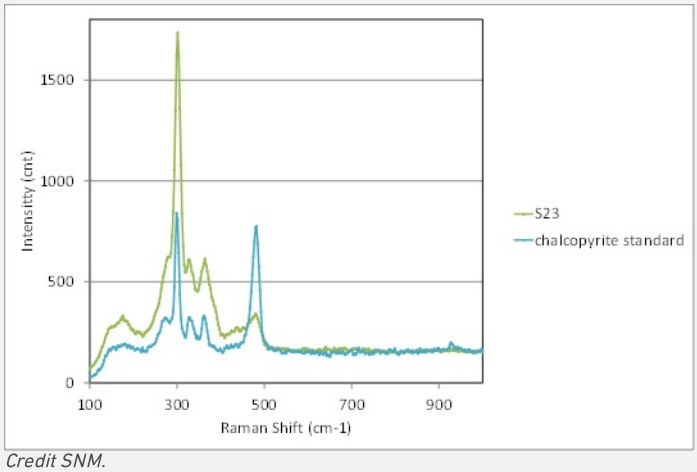

Credit SNM.

Fig. 18: Raman spectrum of the outermost layer (S23) of Fig.14 compared to a chalcopyrite standard spectrum. Settings: laser wavelength 532nm, acquisition time 50s, 4 accumulations, filter D2 (0.75-0.8mW), hole 1000, slit 100, grating 600. Method of analysis: Raman spectroscopy, Lab of Swiss National Museum, Affoltern a. Albis ZH,

Fig. 19: Raman spectrum of the inclusions of the outermost layer (S42) of Fig. 14 compared to a covelline / covellite standard spectrum. Settings: laser wavelength 532nm, acquisition time 10s, 5 accumulations, D2 (0.75-0.8mW), hole 500, slit 80, grating 600. Method of analysis: Raman spectroscopy, Lab of Swiss National Museum, Affoltern a. Albis ZH,

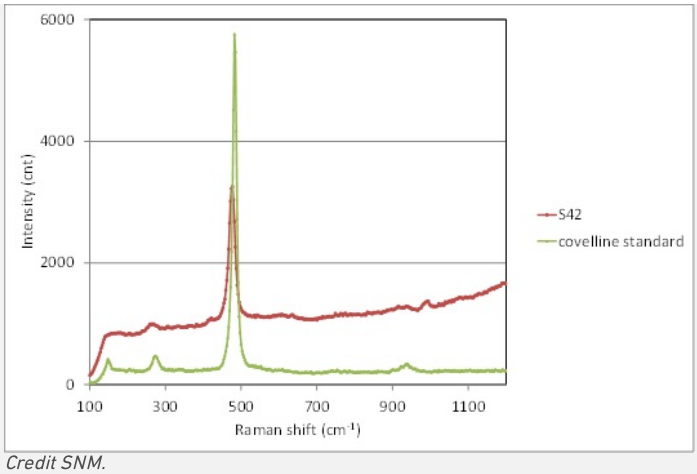

Credit SNM.

Corrosion form	Passive
Corrosion type	lake patina (Schweizer 1994)

Complementary information

Schweizer (1994) indicates that CP1 shows evidence of pseudomorphic replacement of metal grains by corrosion products that we did not observe.

MiCorr stratigraphy(ies) – CS

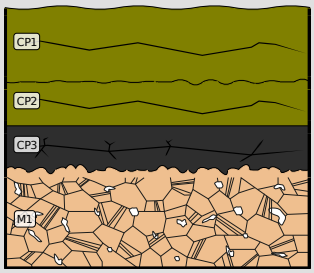

Fig. 20: Stratigraphic representation of the sample taken from the pin without head in cross-section (dark field) using the MiCorr application. The characteristics of the strata are only accessible by clicking on the drawing that redirects you to the search tool by stratigraphy representation. This representation can be compared to Fig. 15, Credit HE-Arc CR.

Synthesis of the binocular / cross-section examination of the corrosion structure

CP1 in binocular mode is documented as CP1 and CP2 in cross-section mode.
CP2 in binocular mode is not observed in cross-section mode, as the observation was made over an area where this layer is absent.
CP3 in binocular mode matches CP3 in cross-section mode.
On cross-section, it was possible to describe and analyze the microstructure of the metal.

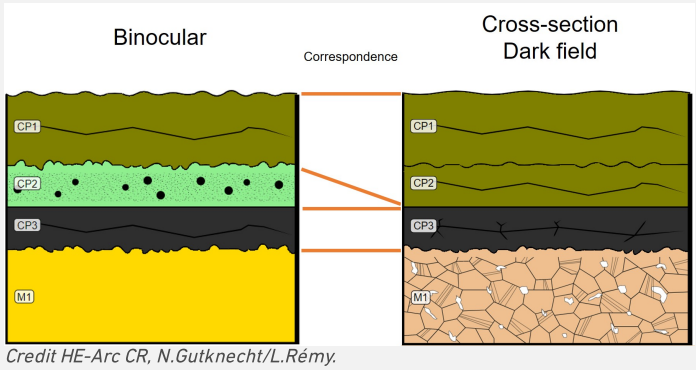

Credit HE-Arc CR, N.Gutknecht/L.Rémy.

Fig. 21: Stratigraphic representation side by side of binocular view and cross-section (dark field),

Conclusion

The pin is made from a tin bronze and has been annealed after cold working. It is covered with a regular, dense brown-yellow corrosion layer, called lake patina by Schweizer (Schweizer, 1994). The inner, thin Sn-rich corrosion layer contains soil elements such as Si. The brown-yellow, thick intermediate and outer corrosion layers have the composition of chalcopyrite. The limit of the original surface can be located between the chalcopyrite and the Cu depleted but Sn-rich inner corrosion layer. The corrosion is a type 1 according to Robbiola et al. 1998. According to Schweizer's research, chalcopyrite can only be generated in the presence of sulfate-reducing bacteria. Conditions for those bacteria are an anaerobic, humid, and S and Fe-rich environment. This object was probably abandoned directly into the lake.

References

References on object and sample

Object files in MiCorr

1. MiCorr_Pin or needle fragment HR-3031
2. MiCorr_Tang fragment of a knife HR-6567
3. MiCorr_Tang fragment of a knife HR-6246
4. MiCorr_Pin HR-17773
5. MiCorr_Pin HR-3071
6. MiCorr_Pin HR-18603
7. MiCorr_Pin HR-3389

References object

8. Rychner-Faraggi A-M. (1993) Hauterive – Champréveyres 9. Métal et parure au Bronze final. Archéologie neuchâteloise, 17 (Neuchâtel).
9. Hochuli, S. et al. (1988) SPM III Bronzezeit , Verlag Schweizerische Gesellschaft für Ur- und Frühgschichte Basel, 76-77, 379.

References sample

10. Empa Report 137 695/1991, P.O. Boll.
11. Rapport d'examen, Lab. Musées d'Art et d'Histoire, Geneva GE, 87-194 à 87-197.
12. Schweizer, F. (1994) Bronze objects from Lake sites: from patina to bibliography. In: Ancient and historic metals, conservation and scientific research (eds. Scott, D.A., Podany, J. and Considine B.B.), The Getty Conservation Institute, 33-50.

References on analytic methods and interpretation

13. Robbiola, L., Blengino, J-M., Fiaud, C. (1998) Morphology and mechanisms of formation of natural patinas on archaeological Cu-Sn alloys, Corrosion Science, 40, 12, 2083-2111.